Synthesis and Antimicrobial Activity of Gold/Silver–Tellurium Nanostructures

ARTICLE *in* ACS APPLIED MATERIALS & INTERFACES · MAY 2014

Impact Factor: 6.72 · DOI: 10.1021/am501134h · Source: PubMed

ACS APPLIED MATERIALS & INTERFACES

Research Article

www.acsami.org

Synthesis and Antimicrobial Activity of Gold/Silver–Tellurium Nanostructures

Hsiang-Yu Chang,[†] Jinshun Cang,[‡] Prathik Roy,[†] Huan-Tsung Chang,*[,†] Yi-Cheng Huang,[§] and Chih-Ching Huang*[,∥,⊥,#]

[†]Department of Chemistry, National Taiwan University, Taipei 10617, Taiwan

[‡]Department of Chemistry, Yancheng Institute of Industry Technology, Yancheng, Jiangsu Province 224005, P. R. China

[§]Department of Food Science, National Taiwan Ocean University, Keelung 20224, Taiwan

[∥]Institute of Bioscience and Biotechnology, National Taiwan Ocean University, Keelung 20224, Taiwan

[⊥]Center of Excellence for the Oceans, National Taiwan Ocean University, Keelung 20224, Taiwan

[#]School of Pharmacy, College of Pharmacy, Kaohsiung Medical University, Kaohsiung, 80708, Taiwan

Supporting Information

ABSTRACT: Gold–tellurium nanostructures (Au–Te NSs), silver–tellurium nanostructures (Ag–Te NSs), and gold/silver–tellurium nanostructures (Au/Ag–Te NSs) have been prepared through galvanic reactions of tellurium nanotubes (Te NTs) with Au^{3+}, Ag^{+}, and both ions, respectively. Unlike the use of less environmentally friendly hydrazine, fructose as a reducing agent has been used to prepare Te NTs from TeO_2 powders under alkaline conditions. The Au/Ag–Te NSs have highly catlaytic activity to convert nonfluorescent Amplex Red to form fluorescent product, revealing their great strength of generating reactive oxygen species (ROS). Au/Ag–Te NSs relative to the other two NSs exhibit greater antimicrobial activity toward the growth of *E. coli*, *S. enteritidis*, and *S. aureus*; the minimal inhibitory concentration (MIC) values of Au/Ag–Te NSs were much lower (>10-fold) than that of Ag–Te NSs and Au–Te NSs. The antibacterial activity of Au/Ag–Te NSs is mainly due to the release of Ag^{+} ions and Te-related ions and also may be due to the generated ROS which destroys the bacteria membrane. *In vitro* cytotoxicity and hemolysis analyses have revealed their low toxicity in selected human cell lines and insignificant hemolysis in red blood cells. In addition, inhibition zone measurements using a Au/Ag–Te NSs-loaded konjac jelly film have suggested that it has great potential in practial application such as wound dressing for reducing bacterial wound infection. Having great antibacterial activitiy and excellent biocompatibility, the low-cost Au/Ag–Te NSs hold great potential as effective antimicrobial drugs.

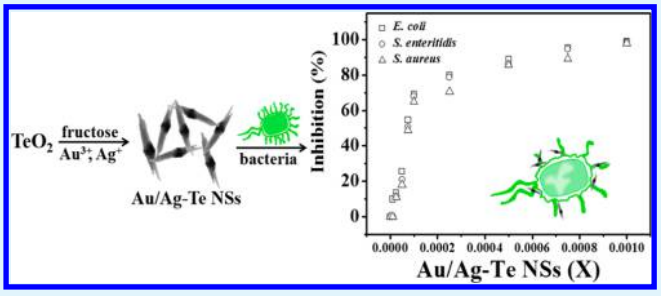

KEYWORDS: *tellurium nanotubes, gold/silver–tellurium nanostructures, galvanic reactions, antimicrobial drugs, reactive oxygen species*

INTRODUCTION

Bacterial infection is a serious public safety issue associated with significant mortality and health-care costs.[1,2] Gram-negative bacteria such as *Escherichia coli* O157:H7 and *Salmonella* and Gram-positive bacteria like *Staphylococcus aureus* have been reported to cause many serious diseases through food and water contaminants.[3,4] Antimicrobial agents such as tetracycline and ampicillin are commonly used to kill or slow the growth of bacteria.[5,6] However, because of broad and often inappropriate use, bacterial resistance to antibacterial drugs may occur.[7] Moreover, administration of high-dose antibiotics may also cause adverse side effects and intolerable toxicity.[8] Thus, developing new and effective antimicrobial drugs is still highly demanded.

Recently, nanomaterials (NMs) have emerged as novel antimicrobial agents.[9−14] The NMs provide many important properties, including generation of a high concentration of free radicals/ions and/or inducing high local temperature during photo-irradiation, release of effective species in the infected area, and/or biocompatibilty. Several classes of antimicrobial nanoparticles (NPs) have proven effective in controlling infection both *in vitro* and *in vivo*, including those which are antibiotic-resistant.[15−20] Compared with conventional antibiotics, antimicrobial NPs have several characteristic advantages, including low acute toxicity, low cost, long-term stability, and easily modifiable surfaces. A particularly unique advantage of NPs with a size smaller than 200 nm is their relatively long circulating half-life, suggesting that they may provide sustained

Received: February 24, 2014
Accepted: May 15, 2014
Published: May 15, 2014

therapeutic effects.[21] Most importantly, antimicrobial NPs can target multiple biological pathways in a wide range of bacteria by compromising the bacterial cell wall/membrane, damaging cellular components through producing reactive oxygen species (ROS), inhibiting enzyme activity and DNA synthesis, and interrupting energy transduction. As a result, the rate at which bacteria are able to develop resistance against the antimicrobial activity of NPs is greatly reduced.

The antimicrobial activity of metallic NPs has been widely studied in human pathogenic bacteria.[15−20] Metallic NPs possess high antimicrobial activity because they release ions and/or induce oxidative strength to kill bacteria or inhibit their growth. Silver (Ag) NPs are currently used in cosmetics, fabrics, and medicine due to their high specificity toward bacterial cells over human cells.[22] The antimicrobial properties of Ag NPs are believed to be associated with the interaction of free silver ions (Ag^+) with negatively charged bacterial membranes that causes membrane rupture and cell lysis.[23] It is also postulated that Ag^+ ions are able to prevent DNA replication and induce inactivation of respiratory enzymes.[24] These particular properties of Ag NPs impart broad-spectrum biocidal effects against both Gram-positive and Gram-negative bacteria, fungi, and viruses as well as some drug-resistant super germs.[25]

Tellurium (Te) compounds have been used as antimicrobial agents in the treatment of infectious diseases (e.g., leprosy, tuberculosis, dermatitis).[26] Recently, numerous synthetic organo-tellurium compounds have been developed for inhibition of bacteria growth.[27,28] For example, nontoxic immunomodulator ammonium trichloro(dioxyethylene-O,Ó)-tellurate (AS101) is used as an inhibitor of cysteine proteases and as a redox modulator of glutathione.[28] Tellurite (TeO_3^{2-}) ions have also been used to inhibit the growth of many microorganisms, particularly penicillin-resistant bacteria.[29,30] The released TeO_3^{2-} ions from Te NMs have been shown effective to kill *E. coli*.[31]

In this work, we prepared antimicrobial gold/silver tellurium nanostructures (Au/Ag−Te NSs). First, we synthesized Te nanotubes (NTs) through a simple fructose-mediated reduction of Te ions in an alkaline aqueous solution.[32] We then prepared three Te-based NMs [Au−Te NSs, Ag−Te NSs, and Au/Ag−Te NSs] from Te NTs through their galvanic reactions with Au^{3+}, Ag^+, and both ions, respectively. The as-prepared Te NMs were thoroughly characterized by conducting transmission electron microscopy (TEM), scanning electron microscopy (SEM), X-ray diffraction (XRD), inductively coupled plasma mass spectrometry (ICP-MS), and X-ray photoelectron spectroscopy (XPS) measurements. The Au/Ag−Te NSs had strong oxidative strength to generate ROS in aqueous solution. Relative to Te NTs, Au−Te NSs, Ag−Te NSs, and Au/Ag−Te NSs possessed superior antimicrobial activity toward *Escherichia coli* (*E. coli*), *Salmonella enterica serovar* Enteritidis (*S. enteritidis*), and *Staphylococcus aureus* (*S. aureus*). The excellent antibacterial properties of Au/Ag−Te NSs are primarily a result of the released Ag^+ and Te-related ions and generated ROS.

EXPERIMENTAL SECTION

Materials. Tellurium dioxide powder (particle size not provided; 99.9%) was purchased from Showa (Tokyo, Japan). D-fructose was purchased from Sigma-Aldrich (St. Louis, MO, USA). Sodium hydroxide pellets were purchased from J. T. Baker (Philipsburg, NJ, USA). Silver nitrate, sodium dodecyl sulfate (SDS), and hydrogen tetrachloroaurate(III) trihydrate ($HAuCl_4{\cdot}3H_2O$) were obtained from Acros (Geel, Belgium). Acetic acid, tris(hydroxymethyl)-aminomethane (Tris), and boric acid were purchased from Mallinckrodt Baker (Phillipsburg, New Jersey, USA). All metallic salts used in this study were purchased from Sigma-Aldrich. Amplex Red (AR) was purchased from Invitrogen (Carlsbad, CA, USA). Fetal bovine serum (FBS) and Roswell Park Memorial Institute (RPMI) 1640 medium were purchased from Gibco BRL (Grand Island, NY, USA). Ampicillin, L-glutamine, and nonessential amino acids were obtained from Biowest (Lewes, UK). Alamar Blue reagent was purchased from BioSource (Camarillo, CA, USA). Sodium phosphate (50 mM, pH 7.0) buffer prepared from phosphoric acid (50 mM) was adjusted with NaOH. Tris-borate (200 mM) buffer was prepared from a 200 mM Tris solution adjusted to pH 7.0 with 500 mM boric acid. Ultrapure water (18.2 MΩ/cm) from a Milli-Q ultrapure water system (Millipore, Billerica, MA) was used throughout the experiments.

Synthesis of Te NTs. Te NTs were prepared using a modified approach according to the literature.[32] In brief, TeO_2 powder (25 mg) was dissolved in NaOH solution (45 mL, 11.11 mM) in a sample vial held in a 60 °C water bath under constant magnetic stirring. After 30 min, 10 M fructose (5 mL, 60 °C) was added to the solution. The solution changed colors from colorless to blue within 5 min, indicating the formation of Te NTs. The solution was diluted 5-fold with 100 mM SDS to terminate the reaction. The sizes of Te NTs were verified to be nearly monodisperse using TEM (Tecnai 20 G2 STwin TEM, Philips/FEI, Hillsboro, Oregon, USA).

Preparation of Te NMs. Prior to use in the preparation of Au and/or Ag hybrid Te NMs (Au−Te NSs, Ag−Te NSs, and Au/Ag−Te NSs), the as-prepared Te NTs were subjected to centrifugation to remove most of the matrix, including SDS and D-fructose. For the sake of simplicity, the concentration of as-purified Te NTs is denoted as 1X. For example, the mixture of 200 μL as-prepared Te NTs (1X) and 800 μL H_2O is denoted as a 0.2X Te NT solution. To prepare Au−Te NSs, Ag−Te NSs, and Au/Ag−Te NSs, aqueous $AgNO_3$, $HAuCl_4$, and $AgNO_3/HAuCl_4$ (each at a final concentration 0.5 mM) were added separately to each of the as-prepared aqueous solutions of Te NTs (0.3X) in a 20 mM Tris-borate solution (pH 7.0). The mixtures were maintained at 25 °C for 1 h and were then subjected to three centrifugation/wash cycles to remove most of the matrix. Centrifugation was performed at a relative centrifugation force (RCF) of 30 000*g* at 4 °C for 15 min, and ultrapure water (1 mL × 3) was used to wash the Te NM pellets.

Characterization of Te NMs. UV−vis absorption spectra of Te NM solutions were recorded using a double-beam UV−vis spectrophotometer (Cintra 10e, GBC, Victoria, Australia). The high-resolution transmission electron microscopy (HRTEM) images of Te NMs were taken on a Tecnai 20 G2 S-Twin TEM (operating at 200 kV). The samples for HRTEM measurements were prepared by placing 10 μL of the Te NM solutions on a carbon-coated copper grid and then dried at room temperature. Chemical identities of Te NMs were determined by energy dispersive X-ray spectroscopy (EDS) analysis using a 0.7-nm-diameter electron probe. XRD samples were prepared by depositing Te NMs on a Si(100) wafer. XRD measurements were performed at room temperature using a Rigaku 18 kW rotating anode source X-ray diffractometer with the Cu Ka1 line (λ = 1.54 Å, energy = 8.8 keV) operated at 50 kV, 100 mA, and slits set at 10 × 2 mm^2. XPS was performed with a PHI 5000 VersaProbe (Physical Electronics, Minnesota, USA) in the constant analyzer energy mode with a pass energy of 28 eV and Al Ka (1486.6 eV) radiation as the excitation source. For determination of the concentrations of metal ions by ICP-MS (Agilent 7700 Series, Agilent Technologies, California, USA), the Te NM samples were prepared in 2% HNO_3.

Oxidative Assay of Te NMs. Aliquots (500 μL) of Tris-borate solutions (5.0 mM, pH 7.0) containing Te NTs, Au−Te NSs, Ag−Te NSs, or Au/Ag−Te NSs (0.1X) were equilibrated with Amplex Red (AR; 50 μM) at room temperature. The mixtures were then left to stand for 2 h prior to fluorescence measurements with an excitation wavelength of 540 nm (Synergy 4 Multi-Mode monochromatic microplate spectrophotometer, Biotek Instruments, Winooski, Vermont, USA).

Bacterial Growth. *E. coli* K12, *S. aureus*, and *S. enteritidis* were grown separately in Luria–Bertani (LB) media [containing bacto-tryptone (2.5 g), bacto-yeast extract (1.25 g), and NaCl (1.25 g) in 250 mL of deionized water]. A single colony of each strain was lifted from LB agar plates and inoculated in LB media (10 mL). The cultures were grown at 37 °C with shaking (200 rpm) until the absorbance value at 600 nm (OD_{600}) reached 1.0 (optical path length = 1.0 cm). A portion of each cell mixture (1.0 mL) was centrifuged (RCF 3000*g*, 10 min, 25 °C) and washed twice with 5.0 mM phosphate buffer solution (pH 7.0) for further use. Bacterial cell suspensions were diluted to obtain 10^4 to 10^5 colony forming units (CFU) mL^{-1}.

Antibacterial Activity. The minimal inhibitory concentrations (MICs) of Te NTs, Au–Te NSs, Ag–Te NSs, and Au/Ag–Te NSs against different bacterial strains were determined using the broth microdilution method.[33] *E. coli*, *S. aureus*, and *S. enteritidis* cells (10^4 cells mL^{-1}) were incubated with fresh Te NTs, Au–Te NSs, Ag–Te NSs, or Au/Ag–Te NSs dispersions (0–4X) in sodium phosphate solutions (5.0 mM, pH 7.0) at 37 °C under shaking at a speed of 250 rpm for 2 h. Cultures were then grown in LB media at 37 °C with shaking (200 rpm) for 16 h. Negative control wells contained only broth or inoculated broth. The bacterial cultures were then serially diluted 10^7-fold, and the cell densities were determined by CFU count on LB agar plates. The inhibitory effect was calculated using the following formula:

$$\text{percent inhibition} = (1 - T/C) \times 100\%$$

where T and C (CFU mL^{-1}) are cell densities of the test and control samples, respectively. Each experiment was performed in duplicate and repeated thrice. The MICs were reported as the lowest concentration of Te NMs capable of completely inhibiting the growth of each bacterial strain tested.

Fluorescence Staining. The bacterial cells were stained with SYTO 9 (6.0 μM) and propidium iodide (PI; 30 μM). Each cell sample treated with Te NTs, Au–Te NSs, Ag–Te NSs, or Au/Ag–Te NSs was then subjected to three centrifugation/wash cycles [centrifuged at RCF 3000*g* for 10 min and washed with 5.0 mM sodium phosphate solution (pH 7.0; 1 mL × 3)] to remove the matrix. The fluorescence images of these treated bacteria were captured using an Olympus BX61 (Tokyo, Japan) microscope with a DP71 digital camera. The fluorescence images of SYTO 9 (green; excitation wavelength, 475 nm; emission wavelength, 530 nm) and PI (red; excitation wavelength, 475 nm; emission wavelength 640 nm) were recorded. The bacteria with green/red fluorescence ratios were used to calculate the percentage of live/dead cells.

Growth Inhibition Zone Determination. To prepare konjac jelly film, 1.6% glucomannan and 0.17% calcium hydroxide were combined at 25 °C, and the mixture was rapidly transferred to a template array (diameter, 8 cm; height, 1 cm). After drying at 60 °C for 12 h, the konjac jelly film was gently washed with ultrapure water (approximately 100 mL) to remove impurities and then dried in the air at room temperature for 6 h prior to use. The Te NM-loaded konjac jelly films were prepared by immersion of konjac jelly films in concentrated 100X Te NMs in 5.0 mM sodium phosphate solution (pH 7.0) for 2 h. Te NMs were self-adsorbed on the jelly films by hydrophobic interactions. After the Te NMs-loaded konjac jelly film was gently washed with ultrapure water (approximately 1 mL) for 30 s to remove any weakly bonded Te NMs or impurities, the jelly film was then dried in the air at room temperature for 2 h prior to use. A well-diffusion method was used to assay the antibacterial activity against test strains on LB agar.[34] A total of 100 μL of diluted inoculum (10^8 CFU mL^{-1}) from *E. coli* suspensions was spread on the surface of the plates to solidify. The jelly films were then cut (diameter, 0.8 cm) and placed onto each of five wells on all plates. After overnight incubation at 37 °C ± 2 °C, the sizes of the zones of inhibition were measured. An unmodified konjac jelly blank was used as a negative control.

***In Vitro* Cytotoxicity.** The human nontumorigenic epithelial cell line (MCF 10A cells), human prostate adenocarcinoma cells (LNCaP cells), human hepatocellular carcinoma cells (HepG2 cells), and human breast cancer cell line (MCF 7 cells) were obtained from American Type Culture Collection (ATCC, Manassas, VA, USA). The cells were cultured in RPMI 1640 supplemented with FBS (10%), ampicillin (1%), L-glutamine (2.0 mM), and nonessential amino acids (1%) in 5% CO_2 at 37 °C. The cell number was determined by the trypan blue exclusion method. Cell viability was determined using an Alamar Blue assay.[35] Following the separate incubation of MCF 10A, LNCaP, HepG2, and MCF 7 cells (approximately 1×10^4 cells/well) in a culture medium for 24 h at 37 °C containing 5% CO_2, each of the culture media was replaced with 100 μL of medium containing Te NTs, Au–Te NSs, Ag–Te NSs, or Au/Ag–Te NSs of different concentrations (0–1.0X). The cells were then incubated for an additional 24 h. The cells were carefully rinsed thrice with phosphate-buffered saline (PBS; pH 7.4, containing 137 mM NaCl, 2.7 mM KCl, 10 mM Na_2HPO_4, and 2.0 mM KH_2PO_4) and treated with Alamar Blue reagent (10-fold dilution, 100 μL/well) for 4 h. Fluorescence due to the reduction of the dye by live cells was measured using a fluorescence microplate reader (Synergy 4), with an excitation wavelength of 545 nm and an emission wavelength of 590 nm. Because fluorescence intensity is directly correlated with cell quantity, cell viability was calculated by assuming 100% viability in the control set (media without Te NMs).

Hemolysis Assays. Hemolysis induced by Te NMs was tested according to a previous report.[36] Fresh blood samples from a healthy volunteer (25 years old) were drawn from the vein into tubes containing ethylenediaminetetraacetic acid (EDTA) and immediately (within 30 min of collection) centrifuged (RCF 3000*g*, 10 min, 4 °C) to remove serum. Fresh red blood cells (RBCs) were then washed thrice with sterile isotonic PBS. Following the last wash, the RBCs were diluted with sterile isotonic PBS to obtain an RBC stock suspension (4 vol % blood cells). The RBC stock suspension (100 μL) was added to each Te NM solution (1X, 0.1X, 0.01X) in 1.5 mL vials. After 1 h of incubation at 37 °C, each of the mixtures was centrifuged at RCF 1000*g* for 10 min. Hemolysis activity was determined by measuring hemoglobin absorption at 576 nm (OD_{576}) in the supernatant (150 μL). Sterile isotonic PBS was used as a reference for 0% hemolysis. One-hundred percent hemolysis was measured by adding ultrapure water to the RBC stock suspension.

$$\text{Hemolysis (\%)} = [(OD_{576\text{TeNMs}} - OD_{576\text{blank}}) / (OD_{576\text{ultrapure water}} - OD_{576\text{blank}})] \times 100$$

RESULTS AND DISCUSSION

Preparation and Characterization of Te NMs. Fructose was used as a reducing and stabilizing agent to prepare Te NTs from TeO_2 in an alkaline solution.[32] The formation of Te NTs by using the present approach was through nucleation and growth steps.[37] First, TeO_2 powder was dissolved in aqueous NaOH solution ($TeO_2 + 2NaOH \rightarrow Na_2TeO_3 + H_2O$), and trigonal Te (t-Te) seeds were recrystallized from the solution by fructose-mediated reduction of TeO_3^{2-}.[32,38] Although fructose itself does not appear to be a reducing agent in solution at pH values around 7.0, it is readily converted to reducing sugars (glucose and mannose) through a keto–enol tautomerism under alkaine conditions.[39] In addition, fructose at high pH values (pH > 10) decomposes to form glyceraldehyde ($HOCH_2CHOHCHO$), which possesses high reducing capability ($HOCH_2CHOHCHO + H_2O \rightarrow HOCH_2CHOHCOOH + 2e^-$, $E^0 = 0.55$ V).[40] Glucose and mannose were not strong enough to reduce TeO_3^{2-} ions to form Te nanomaterials.[32] Therefore, we suggest that the produced glyceraldehyde played a vital role in the fructose-mediated reduction for the preparation of Te NTs. Trigonal Te has a highly anisotropic structure consisting of helical chains of covalently bound Te atoms with three atoms per turn.[38] These chains are held together to form a hexagonal lattice by a combination of electrostatic and van der Waals forces.[41,42] Therefore, the

growth direction is largely confined to the [001] direction, and thus the single crystalline seeds tend to grow into a cylindrical shape.[41,42]

As shown in Figure 1A and Figure S1 (see the Supporting Information), TEM and SEM images clearly reveal that the

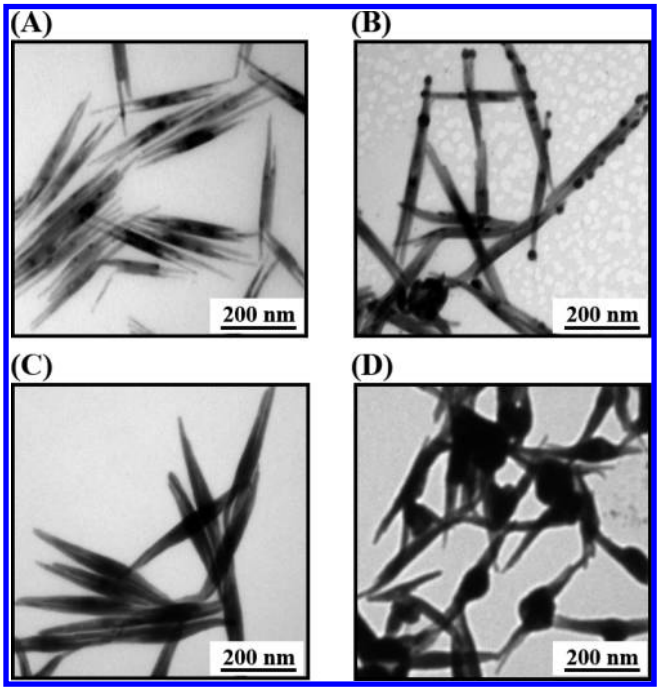

Figure 1. TEM images of the as-prepared (A) Te NTs, (B) Au–Te NSs, (C) Ag–Te NSs, and (D) Au/Ag–Te NSs.

tubular nanostructures of as-prepared Te NTs exhibit hollow interiors with an outer diameter of 25–30 nm and a wall thickness of 5–6 nm. The tubular structures of Te NTs easily form at a low reaction rate. At a high reaction rate, hollow structures are destroyed and solid rod structures emerge.[43] Immediately after the nucleation step, further reduced Te atoms would be preferentially incident at the circumferential edges of each cylindrical seed because these sites relative to the surface have higher free energies.[44,45] As soon as crystal growth started, the concentration of Te atoms near the central portion of this surface became undersaturated, considering the limited mass transport rate in the reaction system. As a result, Te NTs exhibiting well-defined hollow interiors were formed. Cracked structures at the end of as-prepared Te NTs were also observed. The dissolution of Te NTs under alkaline conditions (10 mM NaOH) may be the main reason for the formation of the crack structures at the end of the tubes.

Furthermore, we prepared Au–Te NSs, Ag–Te NSs, and Au/Ag–Te NSs from as-prepared Te NTs in the presence of Au^{3+}, Ag^{+} ions, and both ions, respectively. The galvanic reactions between Au^{3+}/Ag^{+} ions and Te NTs significantly affected the growth rates and facets, leading to the formation of differently structured hybrid Te NMs (Figure 1B–D).[46] The as-prepared Au–Te NSs (Figure 1B) had similar structures to the corresponding Te NTs, and some Au NPs (average size approximately 20 nm) were apparent on the surface of Te NSs (dark parts). The HRTEM image (see Figure S2A of the Supporting Information) of Au–Te NSs reveals an interplanar spacing of 0.23 nm, which corresponds to the lattice planes (111) of the Au structure. The strong galvanic reaction of Te with Ag^{+} led to the formation of long rice-shaped nanostructures (Figure 1C). The interplanar spacing of 0.28 nm (see Figure S2B of the Supporting Information) corresponds to the presence of Ag_2Te in Ag–Te NSs. The selected area electron diffraction (SAED) patterns further reveal that Au (111) and Ag_2Te (220) lattice planes are present in Au–Te NSs and Ag–Te NSs, respectively. Interestingly, when Te NTs reacted with Ag^{+} and Au^{3+}, symmetric dobber-shaped Au/Ag–Te NSs were formed (Figure 1D). Elemental mapping images of Ag, Au, and Te on a single Au/Ag–Te NS (see Figure S3 of the Supporting Information) obtained by high-angle annular dark-field STEM energy-dispersive X-ray (HAADF-STEM-EDX) spectroscopy revealed that Ag and Te were uniformly dispersed on the nanostructure, while Au was only found in the middle area. This result reveals Ag_2Te is the main phase of Au/Ag–Te NSs. Silver can uniformly disperse on the Te nanostructures (see Figure S3 and S4 of the Supporting Information) probably because Ag^{+} has strong hybrid affinity to Te to form Ag_2Te. The cracked structures at the end of Te NSs were not found in Au/Ag–Te NSs, due to dissolution of terminal Te during the reaction. Therefore, gold ions only can be reduced and deposited on the middle area of Te NSs. ICP-MS data showed that the atomic ratio of Au/Te, Ag/Te, and Au/Ag/Te in the as-prepared Au–Te NSs, Ag–Te NSs, and Au/Ag–Te NSs were 1.1/1, 2/1, and 2.5/5/1, respectively.

The absorption bands of Te NTs (Figure 2) at 286 and 616 nm are originated from the energy transfers from the p-bonding

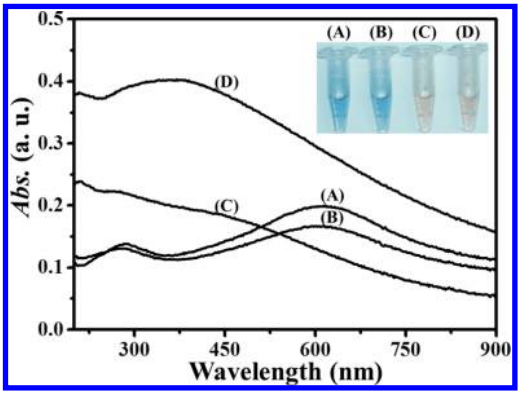

Figure 2. UV–vis absorption spectra of the as-prepared (A) Te NTs, (B) Au–Te NSs, (C) Ag–Te NSs, and (D) Au/Ag–Te NSs in 5.0 mM Tris-borate solution (pH 7.0). Inset: photographic images of the Te NMs solutions.

valence band (VB2) to the p-antibonding conduction band (CB1) and from the p-lone pair valence band (VB3) to the p-antibonding conduction band (CB1) of Te, respectively.[47,48] The absorption spectrum of the Au/Ag–Te NSs is similar to that of Ag–Te NSs. They both exhibit a broad absorption band from 300 to 750 nm. The Au/Ag–Te NSs have a stronger surface plasmon resonance (SPR) absorption in this range due to the formation of a Au nanocomposite in the middle of the NSs. Intense diffraction peaks in the XRD patterns of as-prepared Te NTs and Au/Ag–Te NSs imply good crystallization of the Te NTs (see Figure S4A of the Supporting Information). In addition, the Au/Ag–Te NSs exhibit diffraction peaks of Te (101), Ag_2Te (220), Au (111), Ag_2Te (321), Ag_2Te (404), Ag_2Te (501), Ag_2Te (422), and Au (311) at 2θ values of 27.67, 32.08, 38.02, 46.05, 54.68, 57.35, 67.29,

and 76.85, respectively, revealing a homogenous arrangement of AgTe and Au NPs in Au/Ag−Te NSs (see Figure S4B of the Supporting Information). The slight shift (~0.2°) of the diffraction peak of Au/Ag−Te NSs in Te (101) was probably due to the formation of Ag_2Te that induced some structural defects of Te and a decrease in lattice constants.[49]

Antibacterial Properties of Te NMs. Both Te and Ag have been shown to be effective antimicrobial agents.[22,27−30] Thus, Ag−Te NSs and Au/Ag−Te NSs were expected to possess significantly antibacterial activity. The standard dilution method was used to determine the minimal inhibitory concentration (MIC) values of the as-prepared Te NMs in various tested bacterial strains (Figure 3), including one Gram-

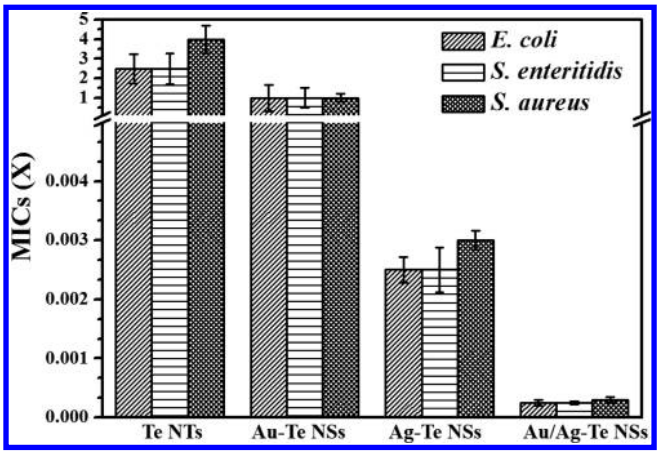

Figure 3. Comparison of minimum inhibitory concentrations (MICs) of tested Te NMs against *E. coli*, *S. enteritidis*, and *S. aureus*. Error bars represent the standard deviation of three repeated measurements.

positive (*S. aureus*) and two Gram-negative (*E. coli* and *S. enteritidis*) bacteria. MIC values of Au/Ag−Te NSs for *E. coli*, *S. enteritidis*, and *S. aureus* were determined to be 0.00025X, 0.00025X, and 0.0003X, respectively. The inhibitory activities of Au/Ag−Te NSs against the three bacterial strains were better than those of Ag−Te NSs (0.0025X/0.0025X/0.003X) and much better than those of Au−Te NSs (1X/1X/1X) and Te NTs (2.5X/2.5X/4X). According to ICP-MS results, the corresponding MIC values (with regard to Ag element) of Au/Ag−Te NSs for the three bacteria (*E. coli*, *S. enteritidis*, and *S. aureus*) were estimated to be 0.14, 0.14, and 0.17 μM (see Figure S5 of the Supporting Information), respectively, which were significantly lower than those of 10 nm Ag NPs (26.0, 26.0, and 39.0 μM) and Ag^+ (5.0, 5.0, and 5.0 μM). The inhibition of different bacteria by Au/Ag−Te NSs (see Figure S6 of the Supporting Information) revealed that Au/Ag−Te NSs only had slightly higher sensitivity toward the Gram-negative bacteria (*E. coli* and *S. enteritidis*) than toward the Gram-positive bacteria (*S. aureus*). *S. aureus* is well known to have much stronger resistance against Ag^+ ions, TeO_3^{2-}, and ROS relative to *E. coli* and *S. enteritidis*.[50] Therefore, we suggest Au/Ag−Te NSs may have stronger interaction with Gram-negative bacteria to destroy bacteria cell membranes. It is noted that each of the Gram-negative bacteria has an outer phospholipidic membrane, whereas each of the Gram-positive bacteria has an outer peptidoglycan layer.[51]

Inhibition zone measurements (see Figure S7 of the Supporting Information) were further conducted to assess the antibacterial activity of Te NTs, Au−Te NSs, Ag−Te NSs, and Au/Ag−Te NSs. Figure S7 reveals that the Au/Ag−Te NS-loaded konjac jelly film exhibited a larger inhibition zone (3.20 ± 0.20 cm) for *E. coli* than those of Te NTs (1.95 ± 0.06 cm), Au−Te NSs (2.15 ± 0.15 cm), and Ag−Te NSs (2.50 ± 0.05 cm). Our results suggest the highly antibacterial Au/Ag−Te NS-loaded konjac jelly films have potential in wound dressing applications for reducing bacterial wound infection. The antibacterial activities of the as-prepared Te nanomaterials (NMs) against *E. coli* were examined using SYTO 9 and PI to stain nucleic acids. The green-fluorescent dye SYTO 9 was able to enter all tested cells, but the red-fluorescent PI was excluded from cells with structurally intact cytoplasmic membranes. Representative micrographs of *E. coli* incubated separately in LB media with and without containing Te NTs, Au−Te NSs, Ag−Te NSs, and Au/Ag−Te NSs are depicted in Figure S8 (see the Supporting Information). The green and red images correspond to live and dead *E. coli*, respectively. The decreasing order of the viability of *E. coli* induced by the Te NMs is Au/Ag−Te NSs > Ag−Te NSs > Au−Te NSs ≅ Te NTs. Taken together, these results reveal that Au/Ag−Te NSs possess superior antibacterial activity compared with other Te NMs.

Antibacterial Mechanism. To understand the antibacterial activities of Au/Ag−Te NSs against bacteria, the ions released from these Te based NMs were investigated by ICP-MS measurements. The ICP-MS data revealed that the concentrations of the released Te-related ions and Ag^+ ions from Ag−Te NSs or Au/Ag−Te NSs were about 0.5 μM and 3.0 μM, respectively, after the bacteria were treated with Ag−Te NSs (0.1X) or Au/Ag−Te NSs (0.1X). Thus, the antibacterial activity of Au/Ag−Te NSs and Ag−Te NSs was strongly related to the release of Ag^+ and Te-related ions. The Te-related ions released from Au/Ag−Te NSs were probably from the surface Te atoms or ions because no significant difference in the size and morphology of Au/Ag−Te NSs was observed after they were dispersed in a bacteria culture medium (LB) for 48 h (data not shown). Although Ag−Te and Au/Ag−Te NSs released similar concentrations of Te-related and Ag^+ ions, the latter had greater antibacterial activity, suggesting some other factors may contribute to the observed high antibacterial activity.

Based on the fact that some NMs possess enzyme-like catalytic activity and can generate ROS,[52−58] the oxidase-like activity of Au/Ag−Te NSs was evaluated using nonfluorescent Amplex Red (AR, 10-acetyl-3,7-dihydroxyphenoxazine) as the substrate in the presence of O_2 (Figure 4).[59] O_2 served as an electron acceptor of the Au/Ag−Te NTs to form highly reactive ROS such as hydroxyl radicals (·OH), H_2O_2, and/or superoxide radical anions ($O_2^{\bullet-}$). These ROS then oxidized AR with a 1:1 stoichiometry to yield a highly colored (extinction coefficient, 54 000 cm^{-1} M^{-1}) and fluorescent (quantum yield, 0.83) resorufin (7-hydroxy-3H-phenoxazin-3-one) through formation of a nonfluorescent AR radical. Two radicals subsequently underwent an enzyme-independent dismutation reaction to form fluorescent resorufin. Te NTs, Au−Te NSs, and Ag−Te NSs exhibited almost no oxidase-like activity for the O_2-mediated AR reaction (the inset of Figure 4). In contrast, the Au/Ag−Te NSs, relative to the Te NMs, induced a 4500-fold higher fluorescence intensity at 585 nm when excited at 540 nm. Various valence states of Au^+/Au^0, Ag^+/Ag^0, and Te^{4+}/Te^0 on the NS surfaces likely accounted for the high oxidase-like activity. The X-ray photoelectron spectra (see Figure S9 of the Supporting Information) of the Au/Ag−Te NSs show an Au $4f_{7/2}$ peak of 84.3 eV between 83.9 (Au^0) and

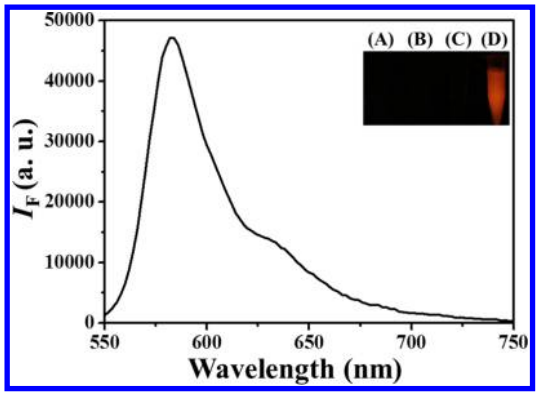

Figure 4. Fluorescence spectrum of Tris-borate solution (5.0 mM, pH 7.0) containing AR (10 μM) and Au/Ag−Te NSs. The excitation wavelength was set at 540 nm. Fluorescence intensity (I_F) is plotted in arbitrary units (a.u.). Inset: fluorescent photographs of Tris-borate solutions (5.0 mM, pH 7.0) containing AR (10 μM) and (A) Te NTs, (B) Au−Te NSs, (C) Ag−Te NSs, or (D) Au/Ag−Te NSs upon excitation under a hand-held UV lamp (365 nm).

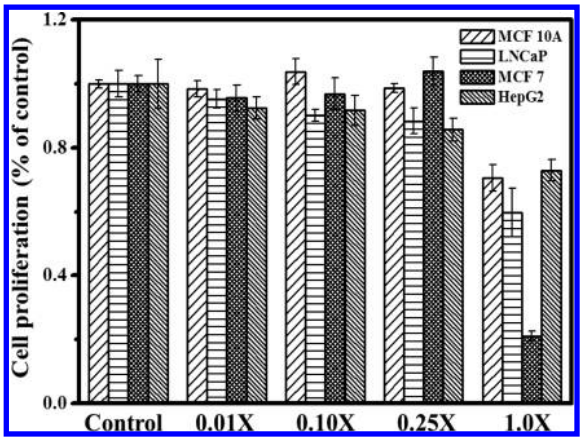

Figure 5. Cell viability of MCF 10A, LNCaP, MCF 7, and HepG2 cells incubated with Au/Ag−Te NSs (at 0.01, 0.10, 0.2,5 and 1.0X) in RPMI-1640 media at 37 °C for 24 h. Isotonic saline solution without Au/Ag−Te NSs was used as a control. Error bars represent the standard deviation of three repeated measurements.

85.0 eV (Au^+) as well as a Ag $3d_{5/2}$ peak of 367.5 eV between 366.7 eV (Ag^0) and 368.3 eV (Ag^+), revealing the coexistence of Au and Ag atoms/ions on the NSs surfaces. In addition to the Te^0 3d binding energy peaks [$3d_{5/2}$ (572.9 eV) and $3d_{3/2}$ (583.8 eV)], signatures of oxidized Te^{4+} peaks were also observed [$3d_{5/2}$ at (576.5 eV) and $3d_{3/2}$ (586.9 eV)]. Au in the Au/Ag−Te NSs plays a vital role in the generation of ROSs that inhibit the growth or kill the bacteria. Au assisted the adsorption of O_2 and increased the electrical conductivity, leading to greater catalytic activity of Au/Ag−Te NSs relative to Ag−Te nanomaterials to produce ROS [e.g., hydroxyl radicals, superoxide radical anions ($O_2^{\bullet-}$), etc.].[54] Possible generation of ROS from chemical and biological reduction of released Te-related ions cannot be ruled out.[60,61] Our results revealed that the high oxidative stress of the Au/Ag−Te NSs-containing solution induced the formation of ROS. The generated ROS may inhibit the bacterial growth through lipid peroxidation and reaction with membrane proteins, DNA, or metabolic enzymes.[56−58,62] Thus, in addition to the released Te-related ions and Ag^+ ions, the generated ROS also contributed the antibacterial activity of Au/Ag−Te NSs.

***In Vitro* Cytotoxicity.** The cytotoxicity of Au/Ag−Te NSs toward mammalian cells was evaluated using an Alamar Blue assay. After 24 h of incubation of MCF 10A, LNCaP, HepG2, and MCF 7 cells with the NMs, we found that the Au/Ag−Te NSs had little influence on cells at low concentration (0.25X; Figure 5) but at a concentration of 1X caused mild toxicity (approximately 20%−70% decreases). Au/Ag−Te NSs therefore demonstrated reasonably good biocompatibility toward mammalian cells, considering the MIC value of the Au/Ag−Te NSs for bacteria is less than 0.0003X. Preferential toxicity to bacterial cells and insignificant cytotoxicity to the mammalian cells insinuate the emergence of Au/Ag−Te NSs as a future putative antimicrobial drug. However, further acute and chronic studies using animal models should be conducted to ensure the potential of Au/Ag−Te NSs as a viable drug.

Hemolysis Assays. Currently, antibiotic treatment is widely used in blood-related therapy to suppress bacterial growth. Therefore, an *in vitro* hemolysis assay was performed to verify satisfactory biocompatibility of Te NMs. The hemolysis assay was performed in defibrinated human blood to test the ability of fragile red blood cells (RBCs) to withstand swelling in contact with Te NM solution. After incubation at 37 °C for 1 h, hemolysis of RBCs was observed only in Ag−Te NSs (1X), revealing that the Au/Ag−Te NSs could serve as potentially safe materials to enhance the efficiency of sterilization in blood (Figure 6).

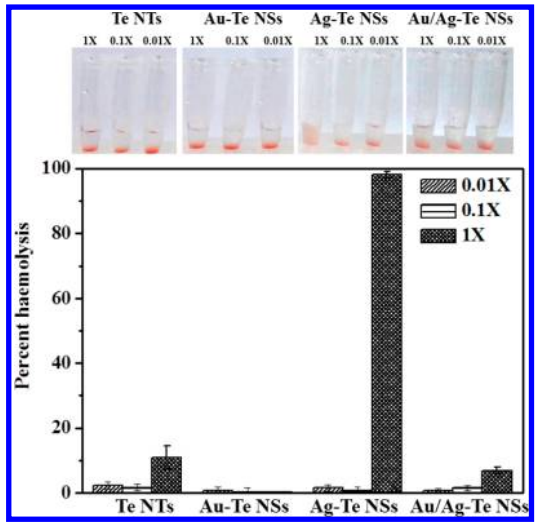

Figure 6. Comparison of hemolytic activities of various Te NMs.

CONCLUSION

In summary, Au/Ag−Te NSs with superior nanoantibiotic properties were prepared through simple galvanic reactions of Te NTs with Au^{3+} and Ag^+ ions at room temperature. Au/Ag−Te NSs exhibited significant antibacterial activity toward both Gram-positive (*S. aureus*) and Gram-negative bacteria (*E. coli* and *S. enteritidis*). The high antibacterial activity for Au/Ag−Te NSs may be ascribed to released Ag^+ ions, Te-related ions, and also the tubular-like NSs and generated ROS that destory the cell membranes. The highly antibacterial Au/Ag−Te NS-loaded konjac jelly film could be used as a wound dressing material for reducing bacterial wound infection. Moreover, the cell viability results showed that Au/Ag−Te NSs had lower toxicity toward human cells and insignificant hemolysis in RBCs. Given the advantages of strong antibacterial activity and low toxicity

against human cells, Au/Ag−Te NSs have great potential as nanoantibiotic agents.

■ ASSOCIATED CONTENT

Supporting Information

Additional information (Figures S1−S9) as noted in the text. This material is available free of charge via the Internet at http://pubs.acs.org/.

■ AUTHOR INFORMATION

Corresponding Authors

*Tel. and fax: 011-886-2-3366-1171. E-mail: changht@ntu.edu.tw.

*Tel.: 011-886-2-2462-2192 ext: 5517. Fax: 011-886-2-2462-2034. E-mail: huanging@ntou.edu.tw.

Notes

The authors declare no competing financial interest.

■ ACKNOWLEDGMENTS

This study was supported by the National Science Council of Taiwan under contracts NSC 101-2113-M-002-002-MY3 and 101-2628-M-019-001-MY3. The assistance of Ms. Ya-Yu Yang and Ms. Ching-Yen Lin from the Instrument Center of National Taiwan University (NTU) for TEM measurement is appreciated. Thanks to Ms. Su-Jen Ji from Precious Instrument Center (National Taiwan University) for assistance in SEM experiments.

■ REFERENCES

(1) Björkhem-Bergman, L.; Bergman, P.; Andersson, J.; Lindh, J. D. Statin Treatment and Mortality in Bacterial Infections − A Systematic Review and Meta-Analysis. *PLoS One* **2010**, *5*, e10702.

(2) Proft, T.; Baker, E. N. Pili in Gram-Negative and Gram-Positive Bacteria - Structure, Assembly and their Role in Disease. *Cell. Mol. Life Sci.* **2009**, *66*, 613−635.

(3) Chowdhury, S. Heterotrophic Bacteria in Drinking Water Distribution System: A Review. *Environ. Monit. Assess.* **2012**, *184*, 6087−6137.

(4) Smith, C. H.; Goldman, R. D. *Staphylococcus aureus* Decolonization for Recurrent Skin and Soft Tissue Infections in Children. *Can. Fam. Phys.* **2012**, *58*, 1350−1352.

(5) Bhatia, S.; Gupta, M. 1,3,4-Oxadiazole as Antimicrobial Agents: An Overview. *J. Chem. Pharm. Res.* **2011**, *3*, 137−147.

(6) Daglia, M. Polyphenols as Antimicrobial Agents. *Curr. Opin. Biotechnol.* **2012**, *23*, 174−181.

(7) Rice, L. B. The Clinical Consequences of Antimicrobial Resistance. *Curr. Opin. Microbiol.* **2009**, *12*, 476−481.

(8) Koluman, A.; Dikici, A. Antimicrobial Resistance of Emerging Foodborne Pathogens: Status Quo and Global Trends. *Crit. Rev. Microbiol.* **2013**, *39*, 57−69.

(9) Li, Q.; Mahendra, S.; Lyon, D. Y.; Brunet, L.; Liga, M. V.; Li, D.; Alvarez, P. J. J. Antimicrobial Nanomaterials for Water Disinfection and Microbial Control: Otential Applications and Implications. *Water Res.* **2008**, *42*, 4591−4602.

(10) Hossain, F.; Perales-Perez, O. J.; Hwang, S.; Román, F. Antimicrobial Nanomaterials as Water Disinfectant: Applications, Limitations and Future Perspectives. *Sci. Total Environ.* **2014**, *466-467*, 1047−1059.

(11) Perelshtein, I.; Applerot, G.; Perkas, N.; Grinblat, J.; Gedanken, A. A One-Step Process for the Antimicrobial Finishing of Textiles with Crystalline TiO_2 Nanoparticles. *Chem.—Eur. J.* **2012**, *18*, 4575−4582.

(12) Azam, A.; Ahmed, A. S.; Oves, M.; Khan, M. S.; Habib, S. S.; Memic, A. Antimicrobial Activity of Metal Oxide Nanoparticles Against Gram-Positive and Gram-Negative Bacteria: A Comparative Study. *Int. J. Nanomed.* **2012**, *7*, 6003−6009.

(13) Dhanasekaran, D.; Latha, S.; Saha, S.; Thajuddin, N.; Panneerselvam, A. Biosynthesis and Antimicrobial Potential of Metal Nanoparticles. *Int. J. Green Nanotechnol.: Biomed.* **2011**, *3*, 72−82.

(14) Rizzello, L.; Cingolani, R.; Pompa, P. P. Nanotechnology Tools for Antibacterial Materials. *Nanomedicine* **2013**, *8*, 807−821.

(15) Chen, C.; Gunawan, P.; Lou, X. W.; Xu, R. Silver Nanoparticles Deposited Layered Double Hydroxide Nanoporous Coatings with Excellent Antimicrobial Activities. *Adv. Funct. Mater.* **2012**, *22*, 780−787.

(16) Prasad, T. N. V. K. V.; Kambala, V. S. R.; Naidu, R. A Critical Review on Biogenic Silver Nanoparticles and their Antimicrobial Activity. *Curr. Nanosci.* **2011**, *7*, 531−544.

(17) Sharma, V. K.; Yngard, R. A.; Lin, Y. Silver Nanoparticles: Green Synthesis and their Antimicrobial Activities. *Adv. Colloid Interface Sci.* **2009**, *145*, 83−96.

(18) Hindi, K. M.; Ditto, A. J.; Panzner, M. J.; Medvetz, D. A.; Han, D. S.; Hovis, C. E.; Hilliard, J. K.; Taylor, J. B.; Yun, Y. H.; Cannon, C. L.; Youngs, W. J. The Antimicrobial Efficacy of Sustained Release Silver-Carbene Complex-Loaded L-Tyrosine Polyphosphate Nanoparticles: Characterization, *in Vitro* and *in Vivo* Studies. *Biomaterials* **2009**, *30*, 3771−3779.

(19) Durmus, N. G.; Webster, T. J. Eradicating Antibiotic-Resistant Biofilms with Silver-Conjugated Superparamagnetic Iron Oxide Nanoparticles. *Adv. Healthcare Mater.* **2013**, *2*, 165−171.

(20) Huh, A. J.; Kwon, Y. J. "Nanoantibiotics": A New Paradigm for Treating Infectious Diseases Ising Nanomaterials in the Antibiotics Resistant Era. *J. Control. Release* **2011**, *156*, 128−145.

(21) Moghimi, S. M.; Hunter, A. C.; Murray, J. C. Long-Circulating and Target-Specific Nanoparticles: Theory to Practice. *Pharmacol. Rev.* **2001**, *53*, 283−318.

(22) Knetsch, M. L. W.; Koole, L. H. New Strategies in the Development of Antimicrobial Coatings: The Example of Increasing Usage of Silver and Silver Nanoparticles. *Polymers* **2011**, *3*, 340−366.

(23) Sondi, I.; Salopek-Sondi, B. Silver Nanoparticles as Antimicrobial Agent: A Case Study on *E. coli* as a Model for Gram-Negative Bacteria. *J. Colloid Interface Sci.* **2004**, *275*, 177−182.

(24) Feng, Q. L.; Wu, J.; Chen, G. Q.; Cui, F. Z.; Kim, T. N.; Kim, J. O. A Mechanistic Study of the Antibacterial Effect of Silver Ions on *Escherichia coli* and *Staphylococcus aureus*. *J. Biomed. Mater. Res.* **2000**, *52*, 662−668.

(25) Rai, M.; Yadav, A.; Gade, A. Silver Nanoparticles as a New Generation of Antimicrobials. *Biotechnol. Adv.* **2009**, *27*, 76−83.

(26) Turner, R. J.; Borghese, R.; Zannoni, D. Microbial Processing of Tellurium as a Tool in Biotechnology. *Biotechnol. Adv.* **2012**, *30*, 954−963.

(27) Soni, D.; Gupta, P. K.; Kumar, Y.; Chandrashekhar, T. G. Antibacterial Activity of some Unsymmetrical Diorganyltellurium(IV) Dichlorides. *Indian J. Biochem. Biophys.* **2005**, *42*, 398−400.

(28) Daniel-Hoffmann, M.; Sredni, B.; Nitzan, Y. Bactericidal Activity of the Organo-Tellurium Compound AS101 Against *Enterobacter cloacae*. *J. Antimicrob. Chemother.* **2012**, *67*, 2165−2172.

(29) Pérez, J. M.; Calderón, I. L.; Arenas, F. A.; Fuentes, D. E.; Pradenas, G. A.; Fuentes, E. L.; Sandoval, J. M.; Castro, M. E.; Elías, A. O.; Vásquez, C. C. Bacterial Toxicity of Potassium Tellurite: Unveiling an Ancient Enigma. *PLoS One* **2007**, *2*, e211.

(30) Valdivia-González, M.; Pérez-Donoso, J. M.; Vásquez, C. C. Effect of Tellurite-Mediated Oxidative Stress on the *Escherichia coli* Glycolytic Pathway. *Biometals* **2012**, *25*, 451−458.

(31) Lin, Z.-H.; Lee, C.-H.; Chang, H.-Y.; Chang, H.-T. Antibacterial Activities of Tellurium Nanomaterials. *Chem.—Asian J.* **2012**, *7*, 930−934.

(32) Wei, T.-Y.; Chang, H.-Y.; Huang, C.-C. Synthesis of Tellurium Nanotubes *via* a Green Approach for Detection and Removal of Mercury Ions. *RSC Adv.* **2013**, *3*, 13983−13989.

(33) Andrews, J. M. Determination of Minimum Inhibitory Concentrations. *J. Antimicrob. Chemother.* **2001**, *48*, 5−16.

(34) Wiegand, I.; Hilpert, K.; Hancock, R. E. W. Agar and Broth Dilution Methods to Determine the Minimal Inhibitory Concentration (MIC) of Antimicrobial Substances. *Nat. Protoc.* **2008**, *3*, 163−175.

(35) O'Brien, J.; Wilson, I.; Orton, T.; Pognan, F. Investigation of the Alamar Blue (Resazurin) Fluorescent Dye for the Assessment of Mammalian Cell Cytotoxicity. *Eur. J. Biochem.* **2000**, *267*, 5421−5426.
(36) Liu, L.; Yang, J.; Xie, J.; Luo, Z.; Jiang, J.; Yang, Y. Y.; Liu, S. The Potent Antimicrobial Properties of Cell Penetrating Peptide-Conjugated Silver Nanoparticles with Eexcellent Selectivity for Gram-Positive Bacteria Over Erythrocytes. *Nanoscale* **2013**, *5*, 3834−3840.
(37) Safdar, M.; Zhan, X.; Niu, M.; Mirza, M.; Zhao, Q.; Wang, Z.; Zhang, J.; Sun, L.; He, J. Site-Specific Nucleation and Controlled Growth of a Vertical Tellurium Nanowire Array for High Performance Field Emitters. *Nanotechnology* **2013**, *24*, 185705.
(38) Mayers, B.; Xia, Y. One-Dimensional Nanostructures of Trigonal Tellurium with Various Morphologies can be Synthesized Using a Solution-Phase Approach. *J. Mater. Chem.* **2002**, *12*, 1875−1881.
(39) Angyal, S. J. The Composition of Reducing Sugars in Solution. *Adv. Carbohydr. Chem. Biochem.* **1984**, *42*, 15−68.
(40) Bar-Even, A.; Flamholz, A.; Noor, E.; Milo, R. Rethinking Glycolysis: On the Biochemical Logic of Metabolic Pathways. *Nat. Chem. Biol.* **2012**, *8*, 509−517.
(41) Lin, Z.-H.; Yang, Z.; Chang, H.-T. Preparation of Fluorescent Tellurium Nanowires at Room Temperature. *Cryst. Growth Des.* **2008**, *8*, 351−357.
(42) Qian, H.-S.; Yu, S.-H.; Gong, J.-Y.; Luo, L.-B.; Fei, L.-F. High-Quality Luminescent Tellurium Nanowires of Several Nanometers in Diameter and High Aspect Ratio Synthesized by a Poly (Vinyl Pyrrolidone) − Assisted Hydrothermal Process. *Langmuir* **2006**, *22*, 3830−3835.
(43) Zhu, H.; Zhang, H.; Liang, J.; Rao, G.; Li, J.; Liu, G.; Du, Z.; Fan, H.; Luo, J. Controlled Synthesis of Tellurium Nanostructures from Nanotubes to Nanorods and Nanowires and their Template Applications. *J. Phys. Chem. C* **2011**, *115*, 6375−6380.
(44) Wang, Z.; Wang, L.; Huang, J.; Wang, H.; Pan, L.; Wei, X. Formation of Single-Crystal Tellurium Nanowires and Nanotubes *via* Hydrothermal Recrystallization and their Gas Sensing Properties at Room Temperature. *J. Mater. Chem.* **2010**, *20*, 2457−2463.
(45) Song, J.-M.; Lin, Y.-Z.; Zhan, Y.-J.; Tian, Y.-C.; Liu, G.; Yu, S.-H. Superlong and High-Quality Tellurium Nanotubes: Synthesis, Characterization, and Electrical Property. *Cryst. Growth Des.* **2008**, *8*, 1902−1908.
(46) Lin, Z.-H.; Chang, H.-T. Preparation of Gold-Tellurium Hybrid Nanomaterials for Surface-Enhanced Raman Spectroscopy. *Langmuir* **2008**, *24*, 365−367.
(47) Isomäki, H. M.; von Boehm, J. Optical Absorption of Tellurium. *Phys. Scripta* **1982**, *25*, 801−803.
(48) Wei, T.-Y.; Chang, H.-Y.; Lee, Y.-F.; Hung, Y.-L.; Huang, C.-C. Selective Tellurium Nanowire-Based Sensors for Mercury(II) in Aqueous Solution. *J. Chin. Chem. Soc.* **2011**, *58*, 732−738.
(49) Sawabe, T.; Akiyoshi, M.; Yoshida, K.; Yano, T. Estimation of Neutron-Irradiation-Induced Defect in 3C-SiC from Change in XRD Peak Shift and DFT Study. *J. Nucl. Mater.* **2011**, *417*, 430−434.
(50) Lowy, F. D. Antimicrobial Resistance: The Example of *Staphylococcus aureus*. *J. Clin. Invest.* **2013**, *111*, 1265−1273.
(51) Lambert, P. A. Cellular Impermeability and Uptake of Biocides and Antibiotics in Gram-Positive Bacteria and Mycobacteria. *J. Appl. Microbiol.* **2002**, *92*, 46S−54S.
(52) Wei, H.; Wang, E. Nanomaterials with Enzyme-Like Characteristics (Nanozymes): Next-Generation Artificial Enzymes. *Chem. Soc. Rev.* **2013**, *42*, 6060−6093.
(53) Wang, C.-I; Periasamy, A. P.; Chang, H.-T. Photoluminescent C-dots@RGO Probe for Sensitive and Selective Detection of Acetylcholine. *Anal. Chem.* **2013**, *85*, 3263−3270.
(54) Lien, C.-W.; Chen, Y.-C.; Chang, H.-T.; Huang, C.-C. Logical Regulation of the Enzyme-Like Activity of Gold Nanoparticles by Using Heavy Metal Ions. *Nanoscale* **2013**, *5*, 8227−8234.
(55) Chen, Y.; Cao, H.; Shi, W.; Liu, H.; Huang, Y. Fe-Co Bimetallic Alloy Nanoparticles as a Highly Active Peroxidase Mimetic and Its Application in Biosensing. *Chem. Commun.* **2013**, *49*, 5013−5015.
(56) Lin, Z.-H.; Shih, Z.-Y.; Roy, P.; Chang, H.-T. Preparation of Photocatalytic Au-Ag_2Te Nanomaterials. *Chem.—Eur. J.* **2012**, *18*, 12330−12336.
(57) Applerot, G.; Lellouche, J.; Lipovsky, A.; Nitzan, Y.; Lubart, R.; Gedanken, A.; Banin, E. Understanding the Antibacterial Mechanism of CuO Nanoparticles: Revealing the Route of Induced Oxidative Stress. *Small* **2012**, *8*, 3326−3337.
(58) Li, Y.; Zhang, W.; Niu, J.; Chen, Y. Mechanism of Photogenerated Reactive Oxygen Species and Correlation with the Antibacterial Properties of Engineered Metal-Oxide Nanoparticles. *ACS Nano* **2012**, *6*, 5164−5173.
(59) Mueller, S.; Riedel, H.-D.; Stremmel, W. Determination of Catalase Activity at Physiological Hydrogen Peroxide Concentrations. *Anal. Biochem.* **1997**, *245*, 55−60.
(60) Molina-Quiroz, R. C.; Loyola, D. E.; Muñoz-Villagrán, C. M.; Quatrini, R.; Vásquez, C. C.; Pérez-Donoso, J. M. DNA, Cell Wall and General Oxidative Damage Underlie the Tellurite/Cefotaxime Synergistic Effect in *Escherichia coli*. *PLoS One* **2013**, *8*, e79499.
(61) Molina-Quiroz, R. C.; Muñoz-Villagrán, C. M.; de la Torre, E.; Tantaleán, J. C.; Vásquez, C. C.; Pérez-Donoso, J. M. Enhancing the Antibiotic Antibacterial Effect by Sub Lethal Tellurite Concentrations: Tellurite and Cefotaxime Act Synergistically in *Escherichia coli*. *PLoS One* **2012**, *7*, e35452.
(62) Cabiscol, E.; Tamarit, J.; Ros, J. Oxidative Stress in Bacteria and Protein Damage by Reactive Oxygen Species. *Int. Microbiol* **2000**, *3*, 3−8.